Available online at www.sciencedirect.com
SCIENCE DIRECT®
Journal of Solid State Chemistry 174 (2003) 349–356
JOURNAL OF SOLID STATE CHEMISTRY
http://elsevier.com/locate/jssc

Temperature-dependent diffraction studies on the phase evolution of tetraindium heptabromide

Michael Scholten, Philipp Kölle, and Richard Dronskowski*

Institut für Anorganische Chemie, Rheinisch-Westfälische Technische Hochschule, Prof.-Pirlet-Strasse 1, D-52056 Aachen, Germany

Received 29 January 2003; received in revised form 14 April 2003; accepted 25 April 2003

Abstract

The mixed-valent compound In_4Br_7 undergoes a higher-order phase transition below 250 K which leads to a decrease in symmetry from the trigonal ($R\bar{3}m$) to the monoclinic ($C2/c$) system via $R\bar{3}c$. The phase transition has been monitored by X-ray powder diffraction using a linear position-sensitive detector between 15 and 300 K, and the crystal structures at room temperature and at 90 K have been refined by means of time-of-flight neutron powder-diffraction data; at 90 K, the lattice parameters are $a = 13.066(1)$ Å, $b = 7.520(1)$ Å, $c = 31.105(1)$ Å, and $\beta = 98.20(1)^\circ$; the new unit cell contains 88 atoms ($Z = 8$) of which 12 are symmetry-independent. Due to their electronic instability because of a second-order Jahn–Teller effect, two of the three crystallographically independent monovalent indium cations are severely affected by the phase transition with respect to their coordination spheres; bond-valence calculations reveal significant strengthening of In^+–Br^- bonding upon symmetry reduction. Structural changes and group–subgroup relationships as well as possible intermediate phases are discussed.

Keywords: Indium bromide; Crystal structure; Phase transition; Powder diffraction; Jahn–Teller distortion

1. Introduction

Within the binary system In/Br, no fewer than seven compounds have been structurally characterized up to now, with In:Br stoichiometric ratios ranging from one (InBr) [1] to three ($InBr_3$) [2]; for an exhaustive compilation, see Ref. [3]. In these compounds, indium adopts the oxidation states one, two, and three. While trivalent indium is exclusively four- or six-coordinated by bromine anions, monovalent indium exhibits an astonishing variety of differing coordinations, with coordination numbers ranging from 7 to 12. The divalent state, on the other hand, occurs in the almost ethane-like dimeric unit $(In_2^{II}Br_6)^{2-}$ [1,2,4].

When it comes to chemical and physical properties, it is first worthwhile mentioning that low-valent indium bromides are extremely sensitive to oxidation and hydrolysis; furthermore, the title compound In_4Br_7 is sensitive to light and mechanical stress. A case of polymorphism in a low-valent indium bromide has been previously reported for In_5Br_7 by Ruck and Bärnighausen [5]. All these phenomena are strongly related with the exceptionally weak In^+–Br^- bonding and the soft interatomic potential [6,7] arising from a second-order Jahn–Teller instability due to the doubly-filled 5*s* atomic orbital on In^+. As a structural consequence of this electronic situation, crystallographic studies have often found exceptionally large values for the In^+ atomic displacement parameters together with empirical bond-valence sums well below one.

The crystal structure of In_4Br_7 is rich in complexity given the simple composition. It was first characterized at room temperature not too long ago (1995) on the basis of medium-resolved X-ray powder data, and it contains five crystallographically independent indium cations plus three bromine anions [8]. Thus, the crystal chemical formula is $(In^{3+})_3(In^+)_5(Br^-)_{14}$ and the trigonal unit cell (hexagonal setting) contains six formula units. A look into the crystal structure is given in Fig. 1.

Here, the indium cations are all stacked on top of each other along the hexagonal *c*-axis. While trivalent indium cations are either tetrahedrally or octahedrally coordinated by bromides with In^{3+}–Br^- distances at 2.47 Å (tetrahedron) and 2.67 Å (octahedron), the monovalent indium cations exhibit coordination numbers of either 10—In(3)—or 12—In(4) and In(5)—with

*Corresponding author. Fax: 0241-80-92288.
E-mail address: drons@HAL9000.ac.rwth-aachen.de (R. Dronskowski).

0022-4596/03/$ - see front matter
doi:10.1016/S0022-4596(03)00243-3

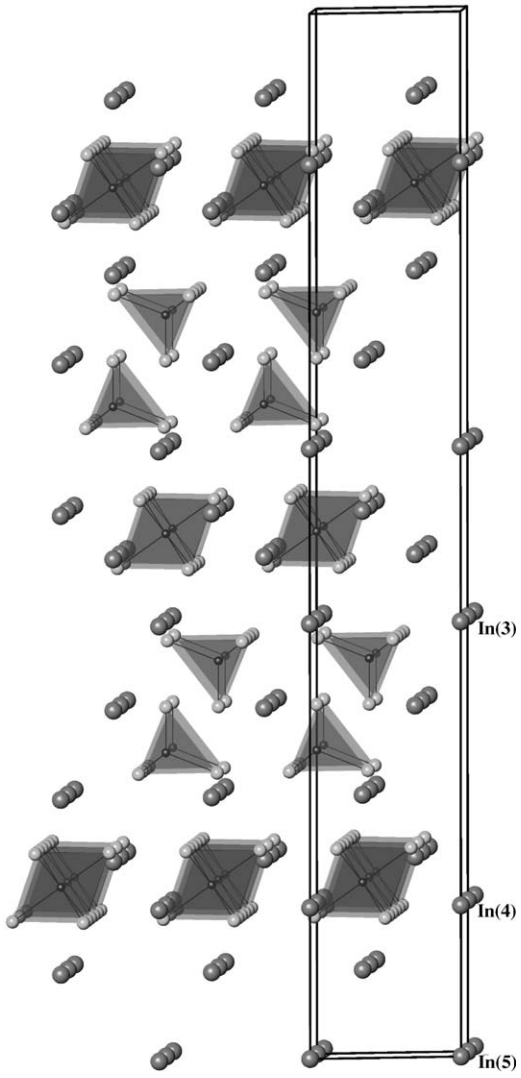

Fig. 1. The crystal structure of trigonal In_4Br_7 at room temperature, with the view perpendicular to the *a*-axis of the trigonal cell (hexagonal setting); see text for atomic labelling.

a wide In^+–Br^- distance spectrum between ca. 3.3 and 4.4 Å.

Already in 1995, a preliminary difference Fourier synthesis based on data taken from an In_4Br_7 crystal cooled to 90 K suggested the possibility of a phase transition at low temperatures, simply due to the second-order Jahn–Teller instability of the monovalent indium atoms, most notably In(5) [8]. This prediction has recently been supported by Yamada and coworkers [9] who investigated several low-valent indium bromides by means of ^{115}In-NMR, ^{115}In-NQR, ^{81}Br-NQR, and also by differential thermal analysis at temperatures between 77 and 370 K. In addition, the authors reported the trigonal phase of In_4Br_7 as being only *metastable* at ambient temperature, changing to an orthorhombic phase over a period of several weeks but reforming upon heating to 420 K. This finding is consistent with our own observation of single crystals of In_4Br_7 decomposing within weeks at room temperature even under argon atmosphere and in complete darkness.

Besides the phase instability of In_4Br_7 mentioned above, two NMR temperature effects were observed at 195 and 95 K. The point-group symmetry of the two different coordination polyhedra around In^{3+} as inferred from ^{81}Br-NQR is in favor of trigonal site symmetry down to 77 K. Recent experimental studies of ours [10,11] on the phase behavior and crystal structure of In_4Br_7 let us now compare our results with the recent, independent nuclear-resonance studies by the Japanese group [9].

2. Experimental

In_4Br_7 was synthesized from indium metal of 99.99% purity (Johnson Matthey) and freshly sublimed $InBr_3$ as has been described before [8]. Single crystals were grown by vacuum sublimation in sealed glass ampoules in the temperature gradient 210/160°C. A plate-like crystal of approximately $0.4 \times 0.4 \times 0.2$ mm^3 was sealed into a glass capillary under argon and mounted on a CAD4 four-circle diffractometer (Enraf Nonius) equipped with monochromatized Mo-$K\alpha$ radiation. The intensities of Bragg reflections were measured at 293 and 220 K.

X-ray powder diffraction patterns at varying temperatures were first recorded on a Guinier diffractometer (Huber G645) with scintillation counter or with a linear position-sensitive detector (Stoe STADI). Time-of-flight (TOF) neutron powder data was recorded at the HRPD diffractometer (ISIS Spallation Source, Rutherford Appleton Laboratory, UK) at 293 and 90 K, and the data from the backscattering bank at 168° in 2θ was used for the refinement. Structure solution was carried out with the SHELXL package [12] while the subsequent Rietveld refinements were done using the programs FULLPROF [13] (X-ray data) and GSAS [14] (neutrons).

3. Results and discussion

To begin with, the known crystal structure of In_4Br_7 at room temperature was independently refined on the basis of high-resolution TOF neutron powder data. An overview of the refinement is shown in Fig. 2 while all important numerical results are given in Table 1 (left part) and Table 2 (atomic positions) and Table 3 (interatomic distances, left part).[1] The new refinement fully corroborates the old X-ray refinement but is

[1] Additional structural details may be obtained from FIZ Karlsruhe, 76344 Eggenstein-Leopoldshafen (Germany), on quoting the depository numbers CSD-412930 (room-temperature phase) and CSD-412931 (low-temperature phase) or directly from R.D.

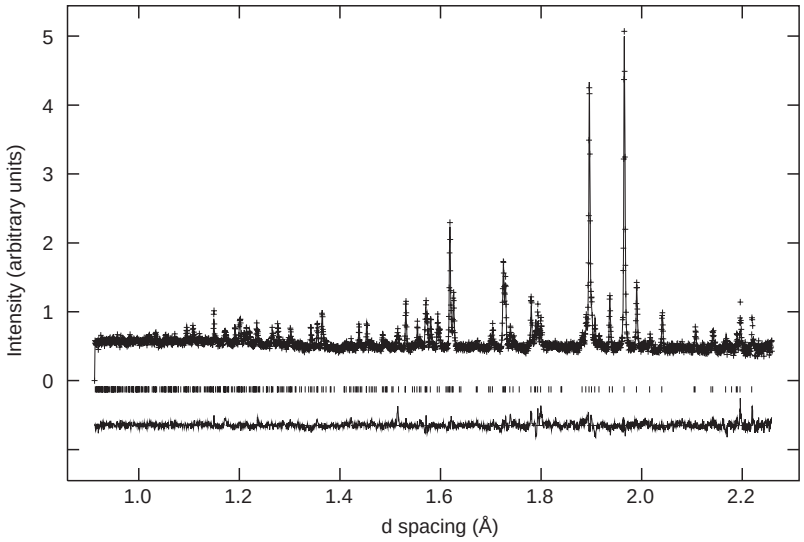

Fig. 2. Time-of-flight neutron Rietveld refinement of the crystal structure of In_4Br_7 at a temperature of 293 K; depicted are (from top to bottom) measured (+) and calculated (line) diffraction patterns, the positions of the Bragg reflections, and the difference between observed and calculated intensities.

Table 1
Crystallographic data of In_4Br_7 at 293 and 90 K

Formula, molar weight:	In_4Br_7; 1018.61 g/mol	
Lattice parameters[a]	$a = 7.583(1)$ Å	$a = 13.066(1)$ Å
		$b = 7.520(1)$ Å
	$c = 46.607(1)$ Å	$c = 31.105(1)$ Å
		$\beta = 98.20(1)^\circ$
Space group, formula units:	$R\bar{3}m$ (no. 166); 6	$C2/c$ (no. 14); 8
Crystallographic density:	4.373 g/cm^3	4.473 g/cm^3
Sample dimension:	$19 \times 31 \times 5$ mm^3 vanadium container	
Instrument:	HRPD Diffractometer (ISIS neutron facility) backscattering bank at 168.33°	
Recording mode:	Time-of-flight	
Range of measurement:	1.037 Å $\leqslant d_{min} \leqslant$ 2.259 Å	0.912 Å $\leqslant d_{min} \leqslant$ 2.486 Å
Measuring temperature:	293(1) K	90(1) K
Number of datapoints, reflections:	3940, 296	3344, 2129
Background:	polynomial, six coefficients	
Refinement method:	Rietveld least-squares	
Profile function:	pseudo-Voigt	
Profile parameters α, β_0, β_1:	0.1157, 0.026(3), 0.000(3)	0.1157, 0.025(3), 0.007(3)
Mixing parameters σ_1, γ_1:	285(17), 32(1)	471(34), 28(2)
Preferred orientation function:	March–Dollase	
Preferred orientation parameter:	$G_1 = 0.800(2)$	$G_1 = 0.858(2)$
Number of variables:	29	57
Number of constraints, restraints:	0, 0	0, 0
R_p; R_{wp}:	0.056; 0.066	0.050; 0.055
$R_{Bragg}(I)$; goodness of fit:	0.132; 1.848	0.061; 1.882

[a] The standard deviations of the lattice parameters have been rounded off to three (lengths) and two (angles) digits. The originally refined (GSAS) lattice parameters were $a = 7.58251(7)$ Å, $c = 46.6070(5)$ Å for 293 K and $a = 13.0660(2)$ Å, $b = 7.5204(1)$ Å, $c = 31.1047(3)$ Å, $\beta = 98.195(1)^\circ$ at 90 K. For the problem of overestimated accuracy in Rietveld refinements, see [15].

characterized by a significantly higher accuracy. The differences between the old and new bond lengths are almost irrelevant, and the only small deviation is related with the bond lengths of the $(In^{III}Br_4)^-$ tetrahedron around In(2) which seems to be a regular one ($4 \times$ 2.45 Å) as opposed to the old X-ray result (1×2.40 Å, 3×2.49 Å).

Also, the highly enlarged displacement parameters of the monovalent indium cations—as well as the one of Br(3)—support the prior X-ray findings. As can be seen

Table 2
Spatial and isotropic displacement parameters of In_4Br_7 at a temperature of 293 K

Atom	Wyckoff site	x	y	z	B_{iso}(Å^2)
In(1)	3*b*	0	0	1/2	2.9(2)
In(2)	6*c*	0	0	0.7094(1)	3.2(2)
In(3)	6*c*	0	0	0.4163(1)	5.7(2)
In(4)	6*c*	0	0	0.1447(2)	9.6(2)
In(5)	3*a*	0	0	0	13.2(5)
Br(1)	18*h*	0.1641(3)	$-x$	0.46704(4)	5.3(8)
Br(2)	18*h*	0.5069(4)	$-x$	0.39545(5)	8.8(1)
Br(3)	6*c*	0	0	0.6568(1)	14.3(3)

Table 3
Interatomic distances (Å) of In_4Br_7 in the trigonal structure at 293 K (left column) and in the monoclinic structure at 90 K (right column) with standard deviations given in parentheses

293 K		90 K	
$In(1)^{3+}$–Br(1)	6 × 2.647(3)	–Br(1)	2 × 2.649(7)
		–Br(2)	2 × 2.674(9)
		–Br(3)	2 × 2.675(8)
$In(2)^{3+}$–Br(3)	1 × 2.452(7)	–Br(4)	1 × 2.47(1)
–Br(2)	3 × 2.452(4)	–Br(5)	1 × 2.49(1)
		–Br(6)	1 × 2.50(1)
		–Br(7)	1 × 2.45(1)
$In(3)^{+}$–Br(1)	3 × 3.200(4)	–Br(1)	1 × 3.19(1)
–Br(3)	1 × 3.407(7)	–Br(2)	1 × 3.19(1)
–Br(2)	6 × 3.915(2)	–Br(3)	1 × 3.18(1)
		–Br(4)	1 × 3.63(1)
		–Br(4)	1 × 4.09(1)
		–Br(5)	1 × 4.17(1)
		–Br(5)	1 × 3.71(1)
		–Br(6)	1 × 3.51(1)
		–Br(6)	1 × 4.32(1)
		–Br(7)	1 × 4.47(1)
$In(4)^{+}$–Br(1)	3 × 3.390(7)	–Br(1)	1 × 3.31(1)
–Br(1)	6 × 3.826(2)	–Br(1)	1 × 3.47(2)
–Br(2)	3 × 4.384(9)	–Br(1)	1 × 4.14(2)
		–Br(2)	1 × 3.33(1)
		–Br(2)	1 × 3.53(2)
		–Br(2)	1 × 4.08(2)
		–Br(3)	1 × 3.39(1)
		–Br(3)	1 × 4.07(2)
		–Br(3)	1 × 3.56(2)
		–Br(4)	1 × 4.13(1)
$In(5)^{+}$–Br(2)	6 × 3.575(3)	–Br(4)	2 × 3.48(1)
–Br(3)	6 × 4.4019(5)	–Br(5)	2 × 3.59(2)
		–Br(6)	2 × 3.50(1)
		–Br(7)	2 × 3.52(2)

from Table 2, the atoms In(5) and Br(3) are most strongly affected, and we reiterate that the 1995 difference Fourier synthesis at 90 K exhibited strangely deformed electron densities in the geometrical plane containing these two atoms.

As a matter of fact, the comparison of two X-ray powder data sets collected at room temperature and close to absolute zero (8 K) indicated a phase transformation. Thus, a 15°-wide fraction of the whole X-ray powder pattern was continuously monitored as a function of the temperature using a linear position-sensitive detector. The resulting T-dependent diffraction pattern is presented in Fig. 3.

The onset of the sought phase transition appears at ca. 250 K by a set of overlapping reflections around 27.9° in 2θ. The gradual increase of the reflection intensities suggests a phase transition of higher order which would appear only as weak slope in a differential thermal analysis. Upon plotting the *combined* X-ray intensities in the above range (27.5–28.3° in 2θ) against the temperature, however, two regions with discontinuities (see Fig. 4) are also visible.

The first, smaller effect is found at a temperature of ca. 190 K, and the second, much more pronounced one, appears at roughly 90 K. The two phenomena show up in both heating and cooling curves, and their reversibility has been assured by performing cooling–heating–cooling sequences. As scattering intensities are not directly related to thermodynamic properties (derivatives of the Gibbs energy function according to which phase transformations are classified), the above anomalies must not be interpreted as transition *points* in terms of a first-order process. There may be more than one process associated with atomic displacements in the crystal lattice, thereby affecting the scattering intensities. The offset between heating and cooling cycles in the figure at 300 K, however, is due to a deliberate intensity offset, and the two curves actually coalesce at that temperature. The above temperatures of discontinuities (190 and 90 K) compare nicely with the two splittings of resonance lines in the ^{81}Br-NQR experiment by Yamada et al., namely 195 and 95 K. Unfortunately, the structural nature of these discontinuities is complicated by the fact that the quality of the data is insufficient for a reliable Rietveld refinement.

Below 250 K, a low-temperature structure solution was then attempted based on X-ray powder data, without success, afterwards using X-ray data collected on a single crystal cooled to 220 K. At that temperature, the latter specimen could not be indexed with the trigonal cell belonging to the room-temperature phase. Instead, a monoclinic unit cell containing eight formula units was found, and the data set was good enough to allow for a structure solution in space group $C2/c$. The subsequent refinements, however, did not converge to exceptionally good R values. This was to be expected since a higher-order phase transition of *klassengleich* type (see below) is inevitably associated with the occurrence of twin domains in the crystal such that some of the reflections must have contributions from more than one of the three possible twin species, and the

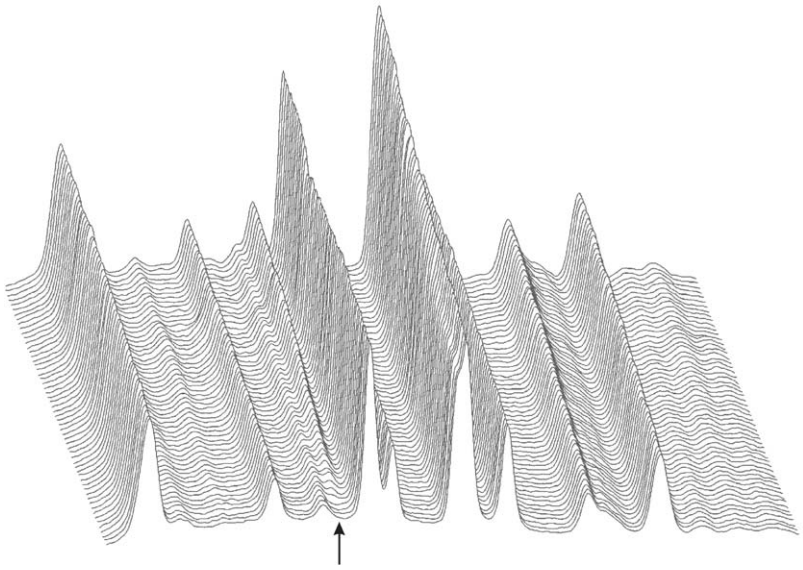

Fig. 3. Phase transition of In_4Br_7 upon cooling as monitored by X-ray diffraction using a linear position-sensitive detector, covering a 2θ range from 22.6 (left) to 37.6° (right). The temperature decreases from the front (300 K) to the back (15 K) in steps of 5 K. Most striking is a set of reflections emerging between 27.5° and 28.3° (arrow); see also Fig. 4.

reflection intensities will be strongly dependent on the degree of overlap of the three domains.

The twin problem, however, can be circumvented if the ultimate refinement of the structure is performed on powder data because the twin components will then be randomly distributed. The monoclinic structure model was therefore refined based on high-resolution TOF neutron powder data recorded at 90 K. An overview of the refinement is shown in Fig. 5 while the corresponding numerical data are given in Table 1 (right part) and Table 4 (atomic positions) and Table 3 (interatomic distances, right part) (see footnote 1). Fig. 6 offers a view of the low-temperature crystal structure.

The refinement's residuals together with the individual standard deviations indicate that the refinement itself is very acceptable despite the high complexity of this binary low-temperature phase. Its structural integrity as proceeding to even lower temperatures was furthermore confirmed by a structural refinement of an independent X-ray diffraction pattern recorded at 8 K. The quality of the latter data set, however, was so low that its details will be omitted for reasons of brevity.

In order to rationalize the structural changes upon phase transition, some features of the above room-temperature phase of In_4Br_7 should be recalled. As listed before in Table 2, there are two trivalent indium cations in tetrahedral and octahedral bromide coordination, respectively, plus three crystallographically different monovalent indium cations, denoted In(3), In(4), and In(5); all indiums reside on special positions. The coordination polyhedra around In(3) with 10 nearest bromine neighbors and around In(4)/In(5) with twelve neighbors are highly symmetric: $In(3)Br_{10}$ and $In(4)Br_{12}$ exhibit site symmetry $3m$ whereas $In(5)Br_{12}$ follows site symmetry $\bar{3}m$.

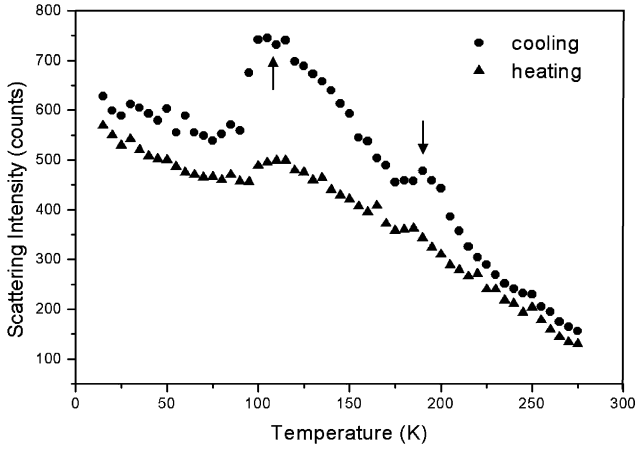

Fig. 4. Integrated X-ray scattering intensity of In_4Br_7 between 27.5° and 28.3° in 2θ with an arbitrary intensity scale; see also Fig. 3.

At room temperature, some of the In^+ and Br^- are subject to exceptionally large displacement parameters, indicating a possible distribution over partially occupied positions of lower site symmetries. The introduction of split atomic positions in the room-temperature phase—e.g., Wyckoff position 6*c* with 50% occupation instead of the fully occupied 3*a* for In(5)—did *not* yield an improved structural model and could therefore not be considered a more accurate description. Nonetheless, even by using the best structural model, bond-valence calculations revealed empirical valences well below one for In(4) and In(5) [8]. All these phenomena are a direct consequence of a second-order Jahn–Teller instability which tend to move the monovalent indiums away from their high-symmetry sites where chemical bonding is

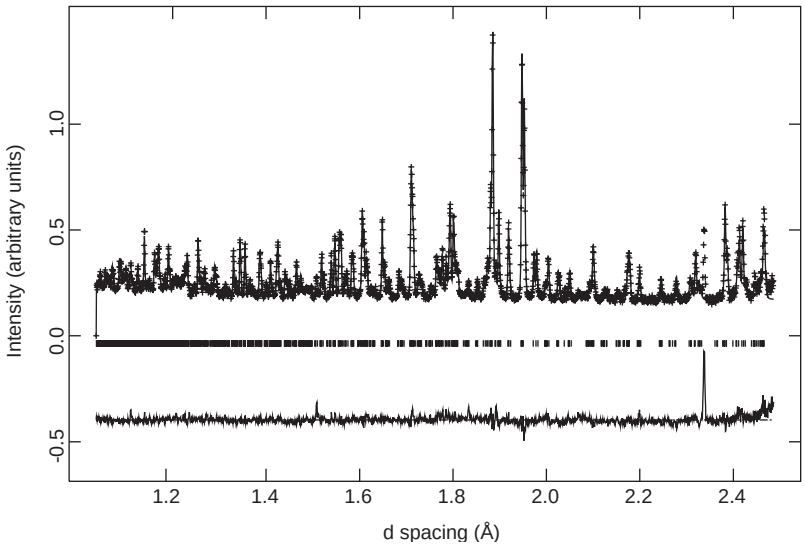

Fig. 5. Same as in Fig. 2 but at a temperature of 90 K. The additional peak showing up at 2.34 Å in the difference signal is caused by the vanadium container.

inadequate. By doing so, an electronic degeneracy present in the highest occupied bands can be removed by mixing a virtual indium 5*p* atomic orbital into the valence region, as shown already from semi-empirical band-structure calculations [8].

Upon cooling, additional degrees of freedom in atomic positions are gained as the collective as well as local symmetry is lowered. Not surprisingly, the bonding of the trivalent indiums to bromine neighbors is not at all affected by the newly adopted crystal structure (see Fig. 6). This finding most notably results from a direct comparison of the In^{3+}–Br^{-} bond lengths of In(1) and In(2) in the low- and room-temperature phase as given in Table 3 (see also discussion of librational motion below). In fact, their coordinations deviate only slightly from ideal tetrahedral and octahedral geometries. This finding is also consistent with the observation of Yamada et al. whose NQR data was compliant with threefold point-group symmetry for In(1) and In(2) even at low temperatures [9].

A sharply contrasting observation holds for the monovalent indium cations. As shown in Fig. 7, there is a large reduction in local symmetry for $In(4)^{+}$ and $In(5)^{+}$ and a much smaller distortion of the polyhedron around $In(3)^{+}$. If In^{+}–Br^{-} bonding is considered up to a distance of 4.5 Å, which has been justified on a theoretical basis [6], coordination numbers lower from 12 to 8 for $In(5)^{+}$, from 12 to 10 for $In(4)^{+}$, but stay constant for 10-coordinate $In(3)^{+}$ (see Fig. 7 and also interatomic distances in Table 3). As a result, highly irregular coordination polyhedra around all In^{+} are found in the monoclinic low-temperature phase because the formerly degenerate electronic symmetry has been broken. The equilibrated electronic situation is nicely mirrored from the course of the well-balanced atomic displacement parameters regardless from the individual atomic types (see Table 4).

Table 4
Spatial and isotropic displacement parameters of In_4Br_7 at a temperature of 90 K

Atom	Wyckoff site	*x*	*y*	*z*	B_{iso} (Å^2)
In(1)	4*d*	1/4	1/4	1/2	2.3(2)
In(2)	8*f*	0.1396(9)	0.776(1)	0.6849(2)	2.4(2)
In(3)	8*f*	0.2093(9)	0.749(2)	0.8741(2)	2.9(2)
In(4)	8*f*	0.068(1)	0.754(2)	0.4686(3)	4.9(2)
In(5)	4*e*	1/2	0.710(3)	3/4	6.2(4)
Br(1)	8*f*	0.1661(1)	0.020(1)	0.5492(2)	3.1(2)
Br(2)	8*f*	0.4317(7)	0.208(1)	0.5506(2)	2.9(1)
Br(3)	8*f*	0.2037(6)	0.518(1)	0.5504(2)	3.3(2)
Br(4)	8*f*	0.0242(5)	0.012(1)	0.6510(2)	3.3(2)
Br(5)	8*f*	0.0674(7)	0.477(1)	0.6627(2)	5.9(2)
Br(6)	8*f*	0.3132(8)	0.805(1)	0.6605(3)	5.7(2)
Br(7)	8*f*	0.1589(8)	0.831(1)	0.7634(2)	6.8(2)

Within a classic crystal-chemical description, the coordination polyhedra around the monovalent indiums are distorted such that In^{+}–Br^{-} bond strength is gained upon cooling. This interpretation can be deduced from simple bond-valence calculations given in Table 5, the parameters having been taken from Ref. [6]. In nice harmony with the above discussion, there is very little change in bond valence sums for the trivalent In(1) and In(2), and also the relatively low-coordinate but monovalent In(3) is not very much affected. The monovalent, formerly 12-coordinate In(4) and In(5), however, increase their valences by about 21% and 40%, respectively, due to a higher differentiation in their coordination shells or, in other words, a lowering of their local symmetries.

The small, *relative decrease* in valences for the trivalent indiums at 90 K, corresponding to wider In^{3+}–Br^{-} distances at lower temperature, is probably unphysical and an artifact of crystallographic description of the 293 K data. If the thermal motions of the atoms belonging to the tetrahedron/octahedron around trivalent In(1)/In(2) are correlated and require a rigid-body approach, the In^{3+}–Br^{-} distances at 293 K (Table 3) are underestimated by ca. 2–3 pm [16]. A numerical, a posteriori correction of these 293 K bond lengths, however, is presently impossible since the powder data do not allow us to refine anisotropic displacement parameters of sufficient quality.

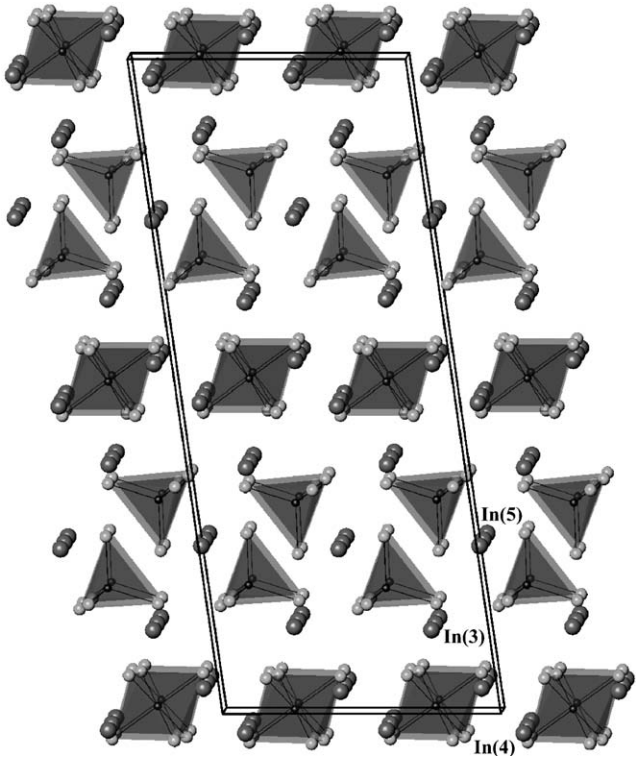

Fig. 6. Same as in Fig. 1 but at a temperature of 90 K. The monoclinic cell is shown perpendicular to the *b*-axis; see also text.

When it comes to the group–subgroup relationship of the phase transformation of In_4Br_7, there are two possible pathways (Fig. 8). The low-temperature cell can either be reached through a trigonal cell with symmetry $R\bar{3}c$ by first doubling the *c*-axis of the former room-temperature cell in $R\bar{3}m$, i.e., in the spirit of a "non-ferroelastic" transition. Although all structural parameters can be derived purely from symmetry considerations, an attempted Rietveld refinement of the low-temperature data using $R\bar{3}c$ symmetry failed; it is straightforward, however, to index all reflections using this particular space-group symmetry! Alternatively, the symmetry reduction from $R\bar{3}m$ to $C2/c$ could proceed via $C2/m$ but it is impossible to derive the corresponding transformation matrices for such a ferroelastic transition. Also, attempts to index the low-temperature data using various transformed monoclinic cells of symmetry $C2/m$ were unsuccessful.

We conclude that all experimental results support the symmetry pathway proceeding via the $R\bar{3}c$ space group. For such a non-ferroelastic transition, one would expect a smaller anomaly in the scattering intensities upon

Table 5
Bond-valence sums *v* of indium cations within In_4Br_7 in the room-temperature and low-temperature crystal structure

Atom	*v* at 293 K	*v* at 90 K	Δ*v* (%)
$In(1)^{3+}$	3.10	2.95	−4.9
$In(2)^{3+}$	3.50	3.27	−6.5
$In(3)^{+}$	1.05	1.03	−1.9
$In(4)^{+}$	0.72	0.87	+20.8
$In(5)^{+}$	0.57	0.80	+40.4

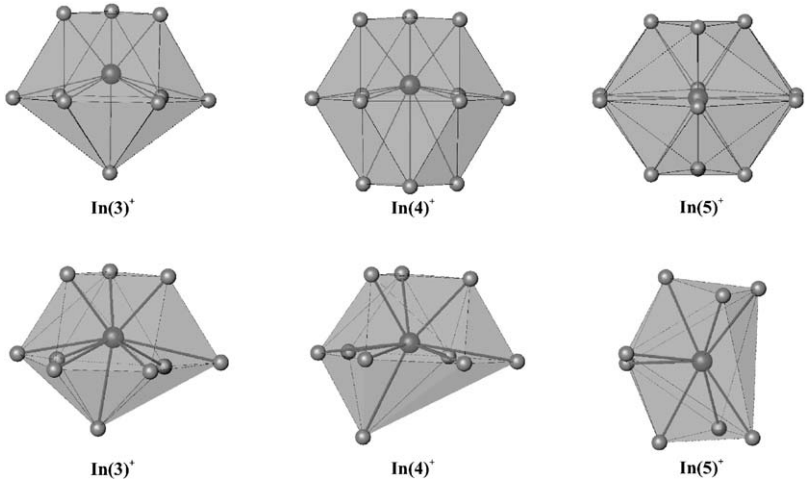

Fig. 7. Structural transformation of the coordination polyhedra around the three monovalent indium cations of In_4Br_7 in going from 293 K (top) to 90 K (bottom).

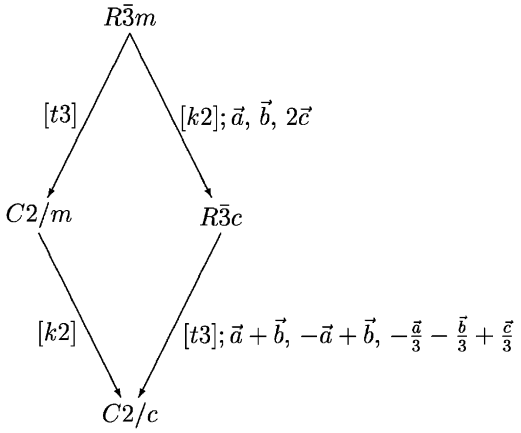

Fig. 8. Group–subgroup relationships between the room-temperature and the low-temperature phase of In_4Br_7, together with the lattice transformations corresponding to the anticipated pathway.

phase transformation, and this is nicely mirrored from the weaker discontinuity observed at $T \approx 190$ K (see again Fig. 4).

4. Conclusion

The evolution of the crystal structure of In_4Br_7 has been investigated by means of temperature-resolved X-ray and neutron diffraction, and the new monoclinic structure of In_4Br_7 at 90 K has been refined from TOF neutron diffraction powder data. The transformation can be described as being higher order although two discontinuities are also observed when going from room temperature down to 15 K. Thus, the present work underpins independent results from nuclear-resonance studies. While the overall symmetry reduction proceeds from trigonal $R\bar{3}m$ (293 K) via $R\bar{3}c$ to monoclinic $C2/m$ (90 K), the phase transition itself is a consequence of the electronic instability of the monovalent indium cations and therefore only affects these, not the trivalent indiums. Thereby, the phase transition has a strong impact on the In^+ coordination by Br^-, eventually leading to significantly strengthened In^+–Br^- bonding. Electronic structure calculations from first principles touching upon the special role of the Jahn–Teller-unstable In^+ are under way.

Acknowledgments

It is a pleasure to thank Drs. Paul Müller and Jürgen Huster for having recorded the X-ray powder patterns. We are also thankful to Dr. Richard Ibberson (ISIS) because of his friendly assistance at the neutron facility and to Professor Theo Hahn (Institut für Kristallographie der RWTH) for insightful suggestions. The continuous financial support by the Fonds der Chemischen Industrie is gratefully acknowledged.

References

[1] T. Staffel, G. Meyer, Z. Anorg. Allg. Chem. 552 (1987) 113.
[2] T. Staffel, G. Meyer, Z. Anorg. Allg. Chem. 563 (1988) 27.
[3] R. Dronskowski, Z. Kristallogr. 210 (1995) 920.
[4] M. Scholten, R. Dronskowski, T. Staffel, G. Meyer, Z. Anorg. Allg. Chem. 624 (1998) 1741.
[5] M. Ruck. H. Bärnighausen, Z. Anorg. Allg. Chem. 625 (1999) 577.
[6] R. Dronskowski, Inorg. Chem. 33 (1994) 6201.
[7] R. Dronskowski, J. Am. Chem. Soc. 117 (1995) 1991.
[8] R. Dronskowski, Angew. Chem. Int. Ed. Engl. 34 (1995) 1126.
[9] K. Yamada, H. Mohara, T. Kubo, T. Imanaka, K. Iwaki, H. Ohkiand, T. Okuda, Z. Naturforsch. A 57 (2002) 375.
[10] M. Scholten, Dissertation, Aachen University of Technology (RWTH), 1998.
[11] Ph. Kölle, Diploma Thesis, Aachen University of Technology (RWTH), 1999.
[12] G.M. Sheldrick, SHELXL-97, a Program for Crystal Structure Determination, University of Göttingen, Germany, 1997.
[13] J. Rodriguez-Carvajal, FULLPROF-2000 (version 1.9), Laboratoire Léon Brillouin, Saclay, France, 2000.
[14] R.B. van Dreele, A. Larson, GSAS, General Structure Analysis System, Los Alamos National Laboratory, 2001.
[15] J.-F. Bérar, P. Lelann, J. Appl. Crystallogr. 24 (1991) 1.
[16] V. Schomaker, K.N. Trueblood, Acta Crystallogr. B 24 (1968) 63.